Higgs boson production at the LHC:

transverse momentum resummation effects in the

$H \rightarrow \gamma\gamma$, $H \rightarrow WW \rightarrow l\nu l\nu$ and $H \rightarrow ZZ \rightarrow 4l$ decay modes

Daniel de Florian[(a,b)], **Giancarlo Ferrera**[(b,c)],
Massimiliano Grazzini[(b)∗] and **Damiano Tommasini**[(b,d)]

[(a)] Departamento de Física, FCEYN, Universidad de Buenos Aires,
(1428) Pabellón 1 Ciudad Universitaria, Capital Federal, Argentina
[(b)]Institut für Theoretische Physik, Universität Zürich, CH-8057 Zürich, Switzerland
[(c)] Dipartimento di Fisica, Università di Milano and
INFN, Sezione di Milano, I-20133 Milan, Italy
[(d)] Dipartimento di Fisica e Astronomia, Università di Firenze and
INFN, Sezione di Firenze, I-50019 Sesto Fiorentino, Florence, Italy

Abstract

We consider Standard Model Higgs boson production through gluon–gluon fusion in hadron collisions. We combine the calculation of the next-to-next-to-leading order QCD corrections to the inclusive cross section with the resummation of multiple soft-gluon emissions at small transverse momenta up to next-to-next-to-leading logarithmic accuracy. The calculation is implemented in the numerical program `HRes` and allows us to retain the full kinematics of the Higgs boson and of its decay products. We present selected numerical results for the signal cross section at the LHC ($\sqrt{s} = 8$ TeV), in the $H \rightarrow \gamma\gamma$, $H \rightarrow WW \rightarrow l\nu l\nu$ and $H \rightarrow ZZ \rightarrow 4l$ decay channels by using the nominal cuts applied in current Higgs boson searches by the ATLAS and CMS collaborations.

March 2012

∗On leave of absence from INFN, Sezione di Firenze, Sesto Fiorentino, Florence, Italy.

1 Introduction

One of the main tasks of the LHC program is the search for the Higgs boson [1] and the study of its properties (mass, couplings, decay widths).

The LHC, after a successful start of pp collisions in 2009 and 2010, has been operated at a centre-of-mass energy of 7 TeV in 2011, and data corresponding to an integrated luminosity of 5.7 fb^{-1} have been accumulated. These data already allowed the ATLAS [2] and CMS [3] experiments to shrink the allowed mass range for the Standard Model (SM) Higgs boson H considerably by essentially excluding the Higgs bosons in the mass range $\mathcal{O}(130 \text{ GeV}) < m_H < \mathcal{O}(600 \text{ GeV})$, while observing an excess of Higgs boson candidate events around $m_H = 125$ GeV. An update of the Tevatron results [4] with up to 10 fb^{-1} integrated luminosity shows a broad excess of events in the region $115-135$ GeV. More data from the LHC 2012 run, that will be operated at a centre-of-mass energy of 8 TeV, are needed to say whether these excesses really correspond to a Higgs signal or are just statistical fluctuations.

In this paper we consider the production of the SM Higgs boson by the gluon fusion mechanism and its decays $H \to \gamma\gamma$, $H \to WW$ and $H \to ZZ$. The gluon fusion process $gg \to H$ [5], through a heavy-quark loop, is the main production mechanism of the SM Higgs boson at hadron colliders. The corresponding cross section is typically at least one order of magnitude larger than the cross section in the other production channels (vector boson fusion, associated production....), and becomes comparable with the cross section for vector boson fusion only at high Higgs boson masses. It is thus essential to achieve reliable theoretical predictions for the gluon fusion cross section and the associated distributions. The dynamics of the gluon fusion mechanism is driven by strong interactions. Thus, accurate studies of the effect of QCD radiative corrections are mandatory to obtain precise theoretical predictions.

The leading order (LO) cross section is proportional to α_S^2, α_S being the QCD coupling. The QCD radiative corrections to the total cross section have been computed at the next-to-leading order (NLO) in Refs. [6, 7, 8] and found to be of the same order as the LO contribution. The next-to-next-to-leading order (NNLO) corrections have been computed in Refs. [9, 10, 11] and their effect is moderate: for a light Higgs, they increases the NLO cross result by about 25% at the LHC ($\sqrt{s} = 8$ TeV). We recall that all the NNLO results have been obtained by using the large-M_t approximation, M_t being the mass of the top quark. Corrections beyond this approximation have been considered in Refs. [12, 13, 14, 15, 16, 17].

The NNLO result mentioned above is certainly important, but it refers to a fully inclusive cross section. The impact of higher-order corrections generally depends on the selection cuts used in the experimental analysis and also the shape of the distributions is typically affected by the applied cuts.

A first step in the direction of taking selection cuts into account was taken in Ref. [18], where the inclusive cross section with a jet veto was computed at NNLO. The first NNLO calculation of the Higgs production cross section that fully takes into account experimental cuts was reported in Ref. [19], in the case of the decay mode $H \to \gamma\gamma$. In Ref. [20] the calculation was extended to the decay mode $H \to WW \to l\nu l\nu$. An independent NNLO calculation of the Higgs production cross section has been presented in Refs. [21, 22], and implemented in the parton-level Monte Carlo program `HNNLO`. Such program allows the user to evaluate the Higgs production cross section with

arbitrary kinematical cuts and includes the decay $H \to \gamma\gamma$, $H \to WW \to l\nu l\nu$ and $H \to ZZ \to 4$ leptons.

Unfortunately, fixed order calculations may suffer from perturbative instabilities when different energy scales are involved. An example is the transverse momentum p_T spectrum of the Higgs boson. In the small-p_T region ($p_T \ll m_H$), the convergence of the fixed-order expansion is spoiled by the presence of large logarithmic terms, $\alpha_S^n \ln^m(m_H^2/p_T^2)$. To obtain reliable predictions, these logarithmically-enhanced terms have to be systematically resummed to all perturbative orders [23]–[32]. It is then important to consistently match the resummed and fixed-order calculations at intermediate values of p_T, in order to obtain accurate QCD predictions for the entire range of transverse momenta. In the case of Higgs boson production the resummation has been performed up to next-to-next-to-leading logarithmic (NNLL) accuracy [33, 31] and matched to the fixed order $\mathcal{O}(\alpha_S^4)$ result valid at large transverse momenta [34, 35, 36]. The calculation has been implemented in a numerical program, named HqT [37] that has been used by the experimental collaborations at the Tevatron and the LHC for a few years. In Ref. [38] the calculation has been extended to include the rapidity dependence of the Higgs boson. In Ref. [39] we have improved the calculation of Ref. [31] by implementing the exact form of the NNLO coefficients of Ref. [40]† and the value for the coefficient $A^{(3)}$ derived in Ref. [41]. The corresponding computation is implemented in a new version of HqT.

In this paper we take one step forward with respect to the work of Refs. [31, 38, 39]. We start from the doubly differential cross section, including transverse-momentum resummation and rapidity dependence [38] and we implement the hard collinear coefficients of Ref. [40] that, together with the exact form of the coefficient $A^{(3)}$ [41], allow us to control the resummation at full NNLL accuracy. We then include the Higgs boson decay and implement the ensuing result into an efficient Higgs event generator, that is able to simulate the full kinematics of the Higgs boson and of its decay products. The resummed result is finally matched with the fixed order NNLO computation of Ref. [21, 22] to obtain a prediction that is everywhere as good as the NNLO result, but includes the resummation of the logarithmically enhanced contributions at small transverse momenta. The exact form of the second order hard-collinear coefficients of Ref. [40] permits a fully consistent matching with the NNLO rapidity distribution upon integration over p_T. The calculation is implemented in a new numerical program called HRes, that embodies the features of HNNLO and HqT. We present a selection of numerical results that can be obtained with our program for Higgs boson production at the LHC ($\sqrt{s} = 8$ TeV) up to NNLL+NNLO accuracy. We consider the decay modes $H \to \gamma\gamma$, $H \to WW \to l\nu l\nu$ and $H \to ZZ \to 4l$ and we compare the resummed results with the corresponding fixed order results, up to the NNLO accuracy, obtained with the HNNLO numerical code.

The paper is organized as follows. In Sect. 2 we recall the main features of our resummation formalism and we introduce our NNLL+NNLO numerical program HRes. In Sect. 3 we present our numerical predictions at the LHC. In Sect. 4 we summarize our results.

---

†The results of Ref. [31, 38] were based on a reasonable approximation of these NNLO hard-collinear coefficients.

2 Transverse momentum resummation and the `HRes` program

We start this Section by briefly recalling the resummation formalism of Refs. [30, 31, 38]. We consider the inclusive hard-scattering process

$$h_1(p_1) + h_2(p_2) \rightarrow H(y, p_T, m_H) + X \quad , \tag{1}$$

where the collision of the two hadrons h_1 and h_2 with momenta p_1 and p_2 produces the Higgs boson H with transverse momentum p_T and rapidity y (defined in the centre-of-mass frame) accompanied by an arbitrary and undetected final state X. The centre-of-mass energy of the colliding hadrons is denoted by $\sqrt{s}$.

According to the QCD factorization theorem, the doubly differential cross section for this process reads

$$\begin{aligned}
\frac{d\sigma}{dy\, dp_T^2}(y, p_T, m_H, s) &= \sum_{a_1, a_2} \int_0^1 dx_1 \int_0^1 dx_2\, f_{a_1/h_1}(x_1, \mu_F^2)\, f_{a_2/h_2}(x_2, \mu_F^2) \\
&\times \frac{d\hat{\sigma}_{a_1 a_2}}{d\hat{y}\, dp_T^2}(\hat{y}, p_T, m_H, \hat{s}; \alpha_S(\mu_R^2), \mu_R^2, \mu_F^2) \ ,
\end{aligned} \tag{2}$$

where $f_{a/h}(x, \mu_F^2)$ $(a = q_f, \bar{q}_f, g)$ are the parton densities of the colliding hadrons at the factorization scale μ_F, $d\hat{\sigma}_{ab}$ are the partonic cross sections, and μ_R is the renormalization scale. The rapidity, $\hat{y}$, and the centre-of-mass energy, $\hat{s}$, of the partonic cross section (subprocess) are related to the corresponding hadronic variables y and s as:

$$\hat{y} = y - \frac{1}{2}\ln\frac{x_1}{x_2} \ , \qquad \hat{s} = x_1 x_2 s \ . \tag{3}$$

The partonic cross section $d\hat{\sigma}_{ab}$ is computable in QCD perturbation theory but its series expansion in α_S contains the logarithmically-enhanced terms, $(\alpha_S^n/p_T^2)\ln^m(m_H^2/p_T^2)$, that we want to resum.

To this purpose, the partonic cross section is rewritten as the sum of two terms,

$$\frac{d\hat{\sigma}_{a_1 a_2}}{d\hat{y}\, dp_T^2} = \frac{d\hat{\sigma}_{a_1 a_2}^{(\text{res.})}}{d\hat{y}\, dp_T^2} + \frac{d\hat{\sigma}_{a_1 a_2}^{(\text{fin.})}}{d\hat{y}\, dp_T^2} \ . \tag{4}$$

The logarithmically-enhanced contributions are embodied in the 'resummed' component $d\hat{\sigma}_{a_1 a_2}^{(\text{res.})}$. The 'finite' component $d\hat{\sigma}_{a_1 a_2}^{(\text{fin.})}$ is free of such contributions, and it can be computed by a truncation of the perturbative series at a given fixed order. In particular we compute $d\hat{\sigma}_{a_1 a_2}^{(\text{fin.})}$ starting from $[d\hat{\sigma}_{a_1 a_2}]_{\text{f.o.}}$, the usual perturbative series truncated at a given fixed order in α_S, and we subtract the perturbative truncation of the resummed component at the same order:

$$\left[\frac{d\hat{\sigma}_{a_1 a_2}^{(\text{fin.})}}{d\hat{y}\, dp_T^2}\right]_{\text{f.o.}} = \left[\frac{d\hat{\sigma}_{a_1 a_2}}{d\hat{y}\, dp_T^2}\right]_{\text{f.o.}} - \left[\frac{d\hat{\sigma}_{a_1 a_2}^{(\text{res.})}}{d\hat{y}\, dp_T^2}\right]_{\text{f.o.}} \ . \tag{5}$$

The resummation procedure of the logarithmic terms has to be carried out [24]-[28] in the impact-parameter space, to correctly take into account the kinematics constraint of transverse-momentum conservation. The resummed component of the partonic cross section is then obtained by performing the inverse Fourier (Bessel) transformation with respect to the impact parameter b. We write[‡]

$$\frac{d\hat{\sigma}_{a_1 a_2}^{(\text{res.})}}{d\hat{y}\, dp_T^2}(\hat{y}, p_T, m_H, \hat{s}; \alpha_{\text{S}}) = \frac{m_H^2}{\hat{s}} \int_0^\infty db\, \frac{b}{2}\, J_0(b p_T)\, \mathcal{W}_{a_1 a_2}(\hat{y}, b, m_H, \hat{s}; \alpha_{\text{S}})\ , \tag{6}$$

where $J_0(x)$ is the 0th-order Bessel function, and the factor $\mathcal{W}$ embodies the all-order dependence on the large logarithms $\ln(m_H^2 b^2)$ at large b, which correspond to $\ln(m_H^2/p_T^2)$ terms in p_T space.

In the case of the p_T cross section integrated over the rapidity, the resummation of the large logarithms is better expressed [30, 31] by defining the N-moments $\mathcal{W}_N$ of $\mathcal{W}$ with respect to $z = m_H^2/\hat{s}$ at fixed m_H. In the present case, in which we want to keep the dependence on the rapidity into account, we consider 'double' (N_1, N_2)-moments with respect to the two variables $z_1 = e^{+\hat{y}} m_H/\sqrt{\hat{s}}$ and $z_2 = e^{-\hat{y}} m_H/\sqrt{\hat{s}}$ at fixed m_H (note that $0 < z_i < 1$). We thus introduce $\mathcal{W}^{(N_1, N_2)}$ as follows [38]:

$$\mathcal{W}_{a_1 a_2}^{(N_1, N_2)}(b, m_H; \alpha_{\text{S}}) = \int_0^1 dz_1\, z_1^{N_1 - 1} \int_0^1 dz_2\, z_2^{N_2 - 1}\, \mathcal{W}_{a_1 a_2}(\hat{y}, b, m_H, \hat{s}; \alpha_{\text{S}})\ . \tag{7}$$

The convolution structure of the QCD factorization formula (2) is easily diagonalized by considering (N_1, N_2)-moments:

$$d\sigma^{(N_1, N_2)} = \sum_{a_1, a_2} f_{a_1/h_1, N_1+1}\, f_{a_2/h_2, N_2+1}\, d\hat{\sigma}_{a_1 a_2}^{(N_1, N_2)}\ , \tag{8}$$

where $f_{a/h, N} = \int_0^1 dx\, x^{N-1} f_{a/h}(x)$ are the customary N-moments of the parton distributions.

The use of Mellin moments also simplifies the resummation structure of the logarithmic terms in $d\hat{\sigma}_{a_1 a_2}^{(\text{res.})\,(N_1, N_2)}$. The perturbative factor $\mathcal{W}_{a_1 a_2}^{(N_1, N_2)}$ can indeed be organized in exponential form as follows:

$$\mathcal{W}^{(N_1, N_2)}(b, m_H; \alpha_{\text{S}}) = \mathcal{H}^{(N_1, N_2)}(m_H, \alpha_{\text{S}}; m_H^2/Q^2)\, \exp\{\mathcal{G}^{(N_1, N_2)}(\alpha_{\text{S}}, \widetilde{L}; m_H^2/Q^2)\}\ , \tag{9}$$

where

$$\widetilde{L} = \ln\left(\frac{Q^2 b^2}{b_0^2} + 1\right)\ , \tag{10}$$

$b_0 = 2 e^{-\gamma_E}$ ($\gamma_E = 0.5772\ldots$ is the Euler number) and, to simplify the notation, the dependence on the flavour indeces has been understood. The scale $Q \sim m_H$ in Eq. (10), named resummation scale, parametrizes the arbitrariness in the resummation procedure. Its role is analogous to the role played by the renormalization (factorization) scale in the context of the renormalization (factorization) procedure. Although the resummed cross section does not depend on Q when evaluated at all perturbative orders, its explicit dependence on Q appears after truncation of the resummed expression at a given logarithmic accuracy.

[‡]In the following equations, the functional dependence on the scales μ_R and μ_F is understood.

The function $\mathcal{H}^{(N_1,N_2)}$ does not depend on the impact parameter b and, therefore, its evaluation does not require resummation of large logarithmic terms. It can be expanded in powers of α_S as

$$\mathcal{H}^{(N_1,N_2)} = \sigma_0(\alpha_S, m_H)\left[1 + \frac{\alpha_S}{\pi}\mathcal{H}^{(N_1,N_2)\,(1)} + \left(\frac{\alpha_S}{\pi}\right)^2\mathcal{H}^{(N_1,N_2)\,(2)} + \dots\right] , \qquad (11)$$

where $\sigma_0(\alpha_S, m_H)$ is the lowest-order partonic cross section for Higgs boson production. The form factor $\exp\{\mathcal{G}\}$ includes the complete dependence on b and, in particular, it contains all the terms that order-by-order in α_S are logarithmically divergent when $b \to \infty$. The functional dependence on b is expressed through the large logarithmic terms $\alpha_S^n \widetilde{L}^m$ with $1 \leq m \leq 2n$. More importantly, all the logarithmic contributions to $\mathcal{G}$ with $n + 2 \leq m \leq 2n$ are vanishing. Thus, the exponent $\mathcal{G}$ can systematically be expanded in powers of α_S, at fixed value of $\lambda = \alpha_S \widetilde{L}$, as follows:

$$\mathcal{G}^{(N_1,N_2)}(\alpha_S, \widetilde{L}; m_H^2/Q^2) = \widetilde{L}\, g^{(1)}(\alpha_S \widetilde{L}) + g^{(2)\,(N_1,N_2)}(\alpha_S \widetilde{L}; m_H^2/Q^2) + \frac{\alpha_S}{\pi}\, g^{(3)\,(N_1,N_2)}(\alpha_S \widetilde{L}; m_H^2/Q^2) + \dots \quad .$$

$$(12)$$

The term $\widetilde{L} g^{(1)}$ collects the leading logarithmic (LL) contributions $\alpha_S^n \widetilde{L}^{n+1}$; the function $g^{(2)}$ includes the next-to-leading logarithmic (NLL) contributions $\alpha_S^n \widetilde{L}^n$; $g^{(3)}$ resums the next-to-next-to-leading logarithmic (NNLL) terms $\alpha_S^n \widetilde{L}^{n-1}$, and so forth.

Note that we use the logarithmic variable $\widetilde{L}$ (see Eq. (10)) to organize the resummation of the large logarithms $\ln(Q^2 b^2)$. In the region in which $Qb \gg 1$ we have $\widetilde{L} \sim \ln(Q^2 b^2)$ and the use of the variable $\widetilde{L}$ is fully legitimate to arbitrary logarithmic accuracy. When $Qb \ll 1$, we have $\widetilde{L} \to 0$ and $\exp\{\mathcal{G}(\alpha_S, \widetilde{L})\} \to 1$. Therefore, the use of $\widetilde{L}$ reduces the effect produced by the resummed contributions in the small-b region (i.e., at large and intermediate values of p_T), where the large-b resummation approach is not justified. In particular, setting $b = 0$ (which corresponds to integrate over the entire p_T range) we have $\exp\{\mathcal{G}(\alpha_S, \widetilde{L})\} = 1$: this property can be interpreted [31] as a unitarity constraint on the total cross section; transverse-momentum resummation smears the shape of the p_T distribution of the Higgs boson without affecting its total production rate.

The resummation formulae (9), (11) and (12) can be worked out at any logarithmic accuracy since the functions $\mathcal{H}$ and $\mathcal{G}$ can be expressed (see Refs. [31, 32]) in terms of few perturbatively-computable coefficients denoted by $A^{(n)}, B^{(n)}, H^{(n)}, C_N^{(n)}, G_N^{(n)}, \gamma_N^{(n)}$. In the case of the p_T cross section integrated over the rapidity, Eq. (9) is still valid, provided the double (N_1, N_2)-moments are replaced by the corresponding single N-moments $\mathcal{W}_N, \mathcal{H}_N, \mathcal{G}_N$ (see Sect. 2.2 in Ref. [31] and Sect. 2 in Ref. [38]).

The formalism briefly recalled in this section defines a systematic expansion [31] of Eq. (4): it can be used to obtain predictions that, formally, have uniform perturbative accuracy from the small-p_T region to the large-p_T region. The various orders of this expansion are denoted as NLL+NLO, NNLL+NNLO, etc., where the first label (NLL, NNLL, ...) refers to the logarithmic accuracy at small p_T and the second label (NLO, NNLO, ...) refers to the customary perturbative order for the inclusive cross section§. To be precise, the NLL+NLO term of Eq. (4) is obtained by including the functions $g^{(1)}$, $g^{(2)}$ [29] and the coefficient $\mathcal{H}^{(1)}$ [42, 43] (see Eqs. (12) and (11)) in the resummed component, and by expanding the finite (i.e. large-p_T) component up to $\mathcal{O}(\alpha_S^3)$.

---

§We note that this notation differs from the one used in Refs. [31, 38, 39], where the various terms of the expansion were denoted by NLL+LO, NNLL+NLO and so forth. Since in this paper we do not limit ourselves to study the Higgs p_T spectrum, we prefer to label the fixed order contributions entering the matching procedure according to the order they contribute to the inclusive cross section.

At NNLL+NNLO accuracy, the resummed component includes also the function $g_N^{(3)}$ [33] and the coefficient $\mathcal{H}^{(2)}$ [40] (see Eqs. (12) and (11)), while the finite component is expanded up to $\mathcal{O}(\alpha_S^4)$. We point out that the NNLL+NNLO (NLL+NLO) result includes the *full* NNLO (NLO) perturbative contribution, supplemented with the resummation of the logarithmically enhanced terms in the small-p_T region at (N)NLL.

In order implement our calculation in a tool that can be used to perform realistic simulations, it is important to consider the Higgs boson decays. Since we are dealing with a scalar particle, the inclusion of the Higgs decay does not lead to substantial complications. However, the efficient generation of "Higgs events" according to the doubly-differential distribution of Eq. (4) and the inclusion of the decay are technically non trivial and require substantial improvements in the speed of the numerical program that evaluates the resummed cross section. The finite part in Eq. (4) is instead evaluated through an appropriate modification of the `HNNLO` code, which being based on the subtraction formalism of Ref. [21], is particularly suitable to this purpose.

We recall [31] that, due to our actual definition of the logarithmic parameter $\widetilde{L}$ in Eq. (9) and to our matching procedure with the perturbative expansion at large p_T, the integral over p_T of the p_T cross section exactly reproduces the customary fixed-order calculation of the total cross section. This integral, however, implies an extrapolation of the resummed result at large transverse momenta, where the resummation cannot improve the accuracy of the fixed order expansion. Moreover, the extrapolation of the resummed cross section at large transverse momenta may lead to unjustified large uncertainties and ensuing lack of predictivity (see Sect. 3 in Ref. [31]). This is not a problem if the calculation is limited to the transverse momentum spectrum. In this case, in fact, we can simply use the fixed order result when the uncertainty of the resummed calculation becomes too large. In the present case, since our goal is to generate the full kinematics of the Higgs boson and its decays without a selection on the Higgs transverse momentum, this issue becomes particularly relevant. In the numerical implementation of Eq. (4) we thus introduce a smooth switching procedure at large p_T, by replacing the resummed cross section in Eq. (4) as follows:

$$\frac{d\hat{\sigma}_{a_1 a_2}}{d\hat{y}\, dp_T^2} \rightarrow w(p_T) \left(\frac{d\hat{\sigma}_{a_1 a_2}^{(\text{res.})}}{d\hat{y}\, dp_T^2} + \frac{d\hat{\sigma}_{a_1 a_2}^{(\text{fin.})}}{d\hat{y}\, dp_T^2} \right) + (1 - w(p_T)) \left[\frac{d\hat{\sigma}_{a_1 a_2}}{d\hat{y}\, dp_T^2} \right]_{\text{f.o.}}. \tag{13}$$

where the function $w(p_T)$ is defined as[¶]

$$w(p_T) = \begin{cases} 1 & p_T \leq p_T^{\text{sw.}} - \Delta p_T \\ f(p_T) & p_T^{\text{sw.}} - \Delta p_T < p_T < p_T^{\text{sw.}} + \Delta p_T \\ 0 & p_T \geq p_T^{\text{sw.}} + \Delta p_T \end{cases} \tag{14}$$

and the function $f(p_T)$ is chosen in such a way that $w(p_T)$ and $w'(p_T)$ are continuous in all the range of transverse momenta. In particular, we choose

$$f(p_T) = \frac{1}{2} \left(\cos\left(\pi \frac{p_T - (p_T^{\text{sw.}} - \Delta p_T)}{2\Delta p_T} \right) + 1 \right). \tag{15}$$

We have checked that the parameters $p_T^{\text{sw.}}$ and Δp_T can be consistently chosen so as not to spoil our unitarity constraint, and that the integral of our NLL+NLO and NNLL+NNLO resummed result still reproduces well the NLO and NNLO inclusive cross sections (see Sec. 3).

[¶] We note that a simpler switching option is available in the new version of `HqT` [37].

We have implemented our calculation in a numerical program called `HRes`, by considering three decay modes: $H \to \gamma\gamma$, $H \to WW \to l\nu l\nu$ and $H \to ZZ \to 4$ leptons. In the latter case the user can choose between $H \to ZZ \to \mu^+\mu^- e^+ e^-$ and $H \to ZZ \to e^+ e^- e^+ e^-$, which includes the appropriate interference contribution. The program can be downloaded from [37], together with some accompanying notes.

3   Results

3.1   Preliminaries

We consider Higgs boson production at the LHC (e.g. pp collisions at $\sqrt{s} = 8$ TeV). In order to avoid a multiple presentation of similar results we use MSTW2008 parton distributions [44], with densities and α_S evaluated at each corresponding order, i.e. we use $(n+1)$-loop α_S at N^nLL+N^nLO and N^nLO (with $n = 1, 2$), and 1-loop α_S for LO. Unless stated otherwise, renormalization, factorization and resummation scales are set to their default values, $\mu_R = \mu_F = 2Q = m_H$. We remind the reader that the calculation is performed in the $M_t \to \infty$ limit.

As for the electroweak couplings, we use the scheme where the input parameters are G_F, m_Z, m_W and $\alpha(m_Z)$. In particular we take $G_F = 1.16639 \times 10^{-5}$ GeV^{-2}, $m_Z = 91.188$ GeV, $m_W = 80.419$ GeV and $\alpha(m_Z) = 1/128.89$. The decay matrix elements are implemented at Born level, i.e., radiative corrections are completely neglected. The Higgs boson is treated in the narrow-width approximation, but in the W and Z decays we take into account finite width effects, by using $\Gamma_W = 2.06$ GeV and $\Gamma_Z = 2.49$ GeV. As explained in Sect. 2, in order to obtain meaningful predictions in the entire range of transverse momenta, we apply a smooth switching procedure (see Eq. (13)). In our numerical implementation the parameters in Eq. (15) are phenomenologically chosen to be $\Delta p_T = 30$ GeV and $p_T^{sw} = a\,m_H + b(m_H/Q + c)\sqrt{s}$. At NLL+NLO accuracy we set $a = 1/2$, $b = 1.2 \times 10^{-3}$ and $c = 2.5$, whereas at NNLL+NNLO we set $a = 0.6$, $b = 2.8 \times 10^{-3}$ and $c = 0$. We postpone some comments on the dependence of our results on these parameters to Sect. 3.5.

3.2 $H \to \gamma\gamma$

We first consider the production of a SM Higgs boson with mass $m_H = 125$ GeV. The width is computed with the program HDECAY [45] to be $\Gamma_H = 4.15$ MeV. With this choice of m_H, the effects of finite width can safely be neglected.

When no cuts are applied, the p_T spectrum of the Higgs boson obtained with `HRes` must be in agreement with the one obtained with the `HqT` numerical program. In Fig. 1 we compare the two spectra to check that this is indeed the case, within the statistical uncertainties. The corresponding inclusive cross sections are reported in Table 1, where we show the new resummed results obtained through the `HRes` code, and we compare them with the fixed order predictions obtained with the `HNNLO` code. We see that the NLL+NLO (NNLL+NNLO) inclusive cross section agrees with the NLO (NNLO) result to better than 1%.
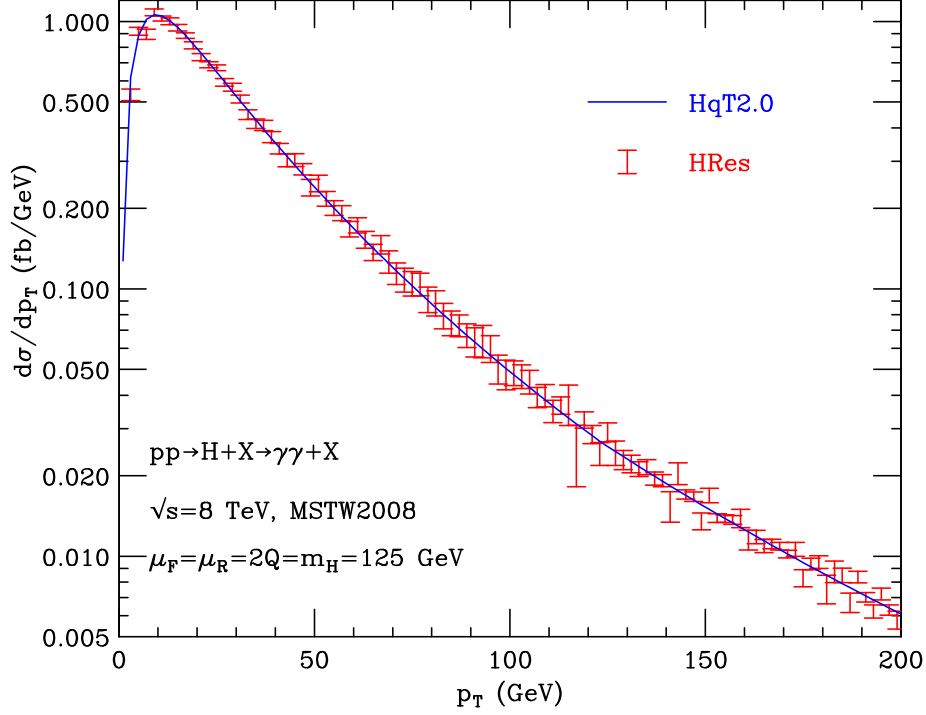
Figure 1: *Transverse momentum spectrum for the $H \to \gamma\gamma$ signal at the LHC for $m_H = 125$ GeV, obtained at NNLL+NNLO with* `HRes` *compared to the corresponding result from* `HqT`. *The result from* `HqT` *is multiplied by the branching ratio* $BR(H \to \gamma\gamma) = 2.245 \times 10^{-3}$ *[45]*.

As an example, we apply the following cuts on the photons. For each event, we classify the photon transverse momenta according to their minimum and maximum value, $p_{T\min}$ and $p_{T\max}$. The photons are required to be in the central rapidity region, $|\eta| < 2.5$, with $p_{T\min} > 25$ GeV and $p_{T\max} > 40$ GeV. Note that an isolation cut on the photons is generally required. For example, a standard isolation is to require the total transverse energy in a cone of a given radius R around each photon to be smaller than a fraction of the photon p_T. Such cuts cannot be taken into account in our resummed calculation, since we are inclusive over the QCD radiation recoiling against the Higgs boson. Their effect can be estimated with the `HNNLO` code and turns out to be rather small.

Cross section	NLO	NLL+NLO	NNLO	NNLL+NNLO
Total [fb]	30.65 ± 0.01	30.79 ± 0.03	38.47 ± 0.15	38.41 ± 0.06
With cuts [fb]	21.53 ± 0.02	21.55 ± 0.01	27.08 ± 0.08	26.96 ± 0.04
Efficiency [%]	70.2	70.0	70.4	70.2

Table 1: *Fixed order and resummed cross sections for* $pp \to H + X \to \gamma\gamma + X$ *at the LHC, before and after geometrical acceptance cuts.*

We recall that the resummation does not affect the total cross section for the Higgs boson production, but when geometrical cuts are applied, their effect can act in a different way on fixed order and resummed calculations. In Table 1 we compare the accepted cross sections, obtained by the fixed order and resummed calculations, and the corresponding efficiencies. The numerical errors estimate the statistical uncertainty of the Monte Carlo integration. Comparing resummed and fixed order predictions, we see that there are no substantial differences on the accepted cross

section, due to the fact that the integration is performed over a wide kinematical range. In Table 2 we report the accepted cross section for different choices of the scales. After selection cuts, the scale uncertainty is about $\pm15\%$ ($\pm18\%$) at NLL+NLO (NLO) and $\pm9\%$ ($\pm10\%$) at NNLL+NNLO (NNLO).

Cross section [fb]	NLO	NLL+NLO	NNLO	NNLL+NNLO
$(2Q = \mu_F = \mu_R) = m_H/2$	25.92 ± 0.02	25.57 ± 0.03	29.52 ± 0.13	29.59 ± 0.11
$(2Q = \mu_F = \mu_R) = m_H$	21.53 ± 0.02	21.55 ± 0.01	27.08 ± 0.08	26.96 ± 0.04
$(2Q = \mu_F = \mu_R) = 2m_H$	18.17 ± 0.01	18.80 ± 0.02	24.43 ± 0.06	24.69 ± 0.06

Table 2: *NLO, NLL+NLO, NNLO and NNLL+NNLO accepted cross sections for $pp \to H + X \to \gamma\gamma + X$ at the LHC, for different choices of the scales.*

In Fig. 2 we study the distribution in the azimuthal separation of the photons in the transverse plane, $\Delta\phi$. At LO the photons are back-to-back, and thus $\Delta\phi$ is 180°. Beyond LO, events with $\Delta\phi$ different from 180° are allowed, but NLO (dots) and NNLO (dashes) results show an unphysical behaviour as $\Delta\phi \to 180^o$. The resummed NLL+NLO and NNLL+NNLO results lead instead to a smooth behaviour in this region. On the other hand, $\Delta\phi \to 0$ corresponds to a kinematical configuration where the diphoton system is produced with large transverse momentum, so the result is fully dominated by the corresponding fixed order calculation.
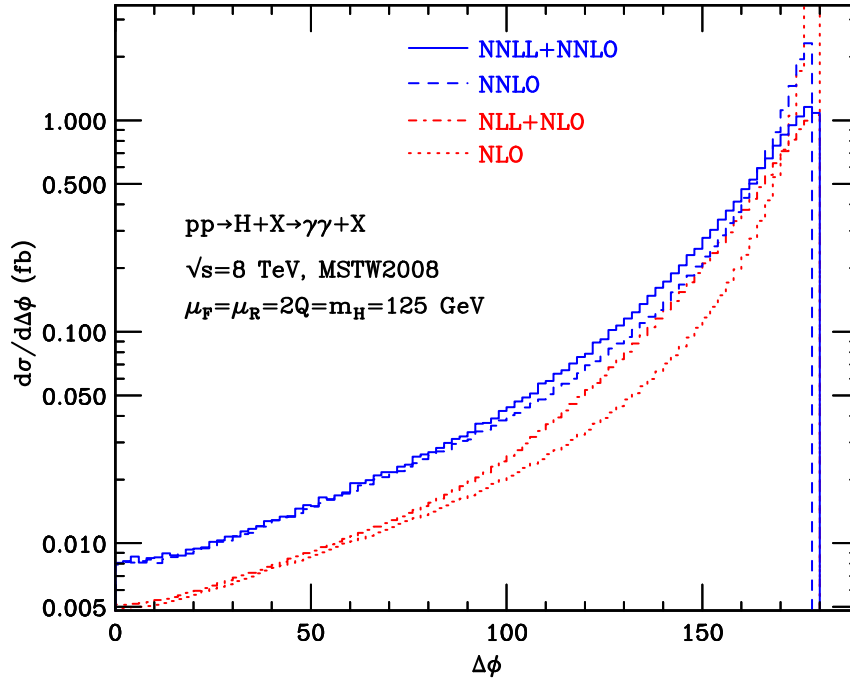

Figure 2: *$\Delta\phi$ distribution from the $H \to \gamma\gamma$ signal at the LHC, obtained by the fixed order and resummed calculation.*

An interesting observable, which has been used by ATLAS to split the $H \to \gamma\gamma$ analysis in categories [46], is the thrust transverse momentum $p_{Tt}^{\parallel}$ [47]. Defining the thrust axis $\hat{t}$ and the

---

$^{\parallel}$In the context of Drell-Yan lepton pair production, this variable is also called a_T [47, 48].

transverse momentum of the diphoton system $\vec{p}_T^{\gamma\gamma}$ as follows

$$\hat{t} = \frac{\vec{p}_T^{\gamma_1} - \vec{p}_T^{\gamma_2}}{|\vec{p}_T^{\gamma_1} - \vec{p}_T^{\gamma_2}|}; \qquad \vec{p}_T^{\gamma\gamma} = \vec{p}_T^{\gamma_1} + \vec{p}_T^{\gamma_2}, \tag{16}$$

the p_{Tt} is then calculated according to:

$$p_{Tt} = |\vec{p}_T^{\gamma\gamma} \times \hat{t}|. \tag{17}$$

In Fig. 3 we report the p_{Tt} distribution, obtained at NLO (dots), NNLO (dashes), NLL+NLO (dot dashes) and NNLL+NNLO (solid). We see that in the high p_{Tt} region the NLL+NLO prediction agrees with the NLO one, and the NNLL+NNLO prediction agrees with NNLO. In the low p_{Tt} region the NLO result diverges to $+\infty$, whereas the NNLO diverges to $-\infty$. Such behaviour is analogous to the behaviour of the p_T distribution of the Higgs boson when computed at fixed order in QCD perturbation theory. The NLL+NLO and NNLL+NNLO results obtained with `HRes` are instead finite as $p_{Tt} \to 0$, approaching a constant value.

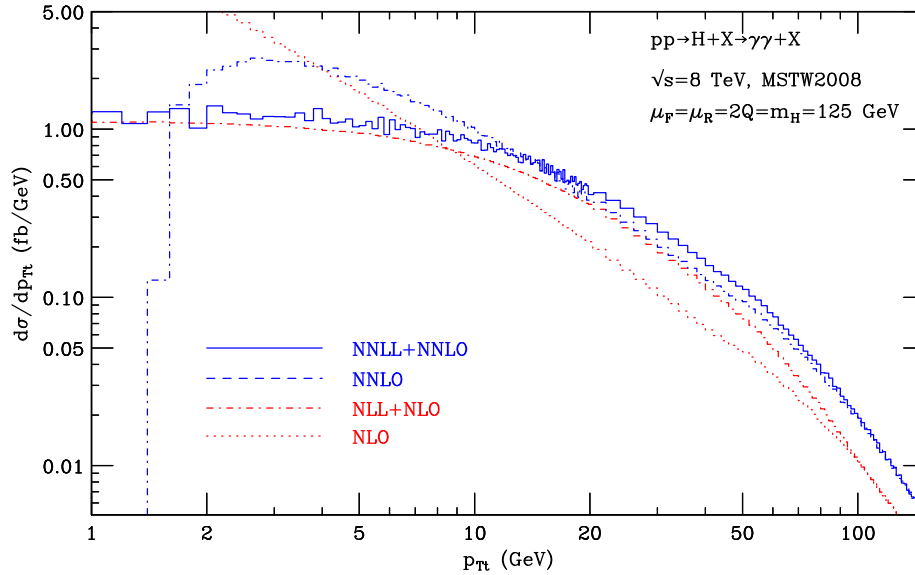Figure 3: *p_{Tt} distribution for the $H \to \gamma\gamma$ signal at the LHC, obtained at NLL+NLO and NNLL+NNLO compared to the corresponding NLO and NNLO results.*

In Fig. 4(a),4(c) we plot the photon p_T distributions $p_{T\min}$ and $p_{T\max}$. These distribution are enhanced when going from LO to NLO to NNLO according to the increase of the total cross section. We note that, as pointed out in Ref. [21], the shape of these distributions sizeable differs when going from LO to NLO and to NNLO. In particular, at the LO the two photons are emitted with the same p_T because the Higgs boson is produced with zero transverse momentum, hence the LO $p_{T\min}$ and $p_{T\max}$ are exactly identical. Furthermore the LO distribution has a kinematical boundary at $p_T = m_H/2$ (Jacobian peak), which is due to the use of the narrow width approximation. Such condition is released once extra radiation is accounted for. Thus higher order predictions suffer of perturbative instabilities, i.e. each higher-order perturbative contribution produces (integrable) logarithmic singularities in the vicinity of that boundary, as explained in Ref. [49].

The same $p_{T\min}$ and $p_{T\max}$ predictions are shown in Fig. 4(b),4(d); in this case the NNLO result is compared with the resummed result at the NLL+NLO and NNLL+NNLO accuracy.
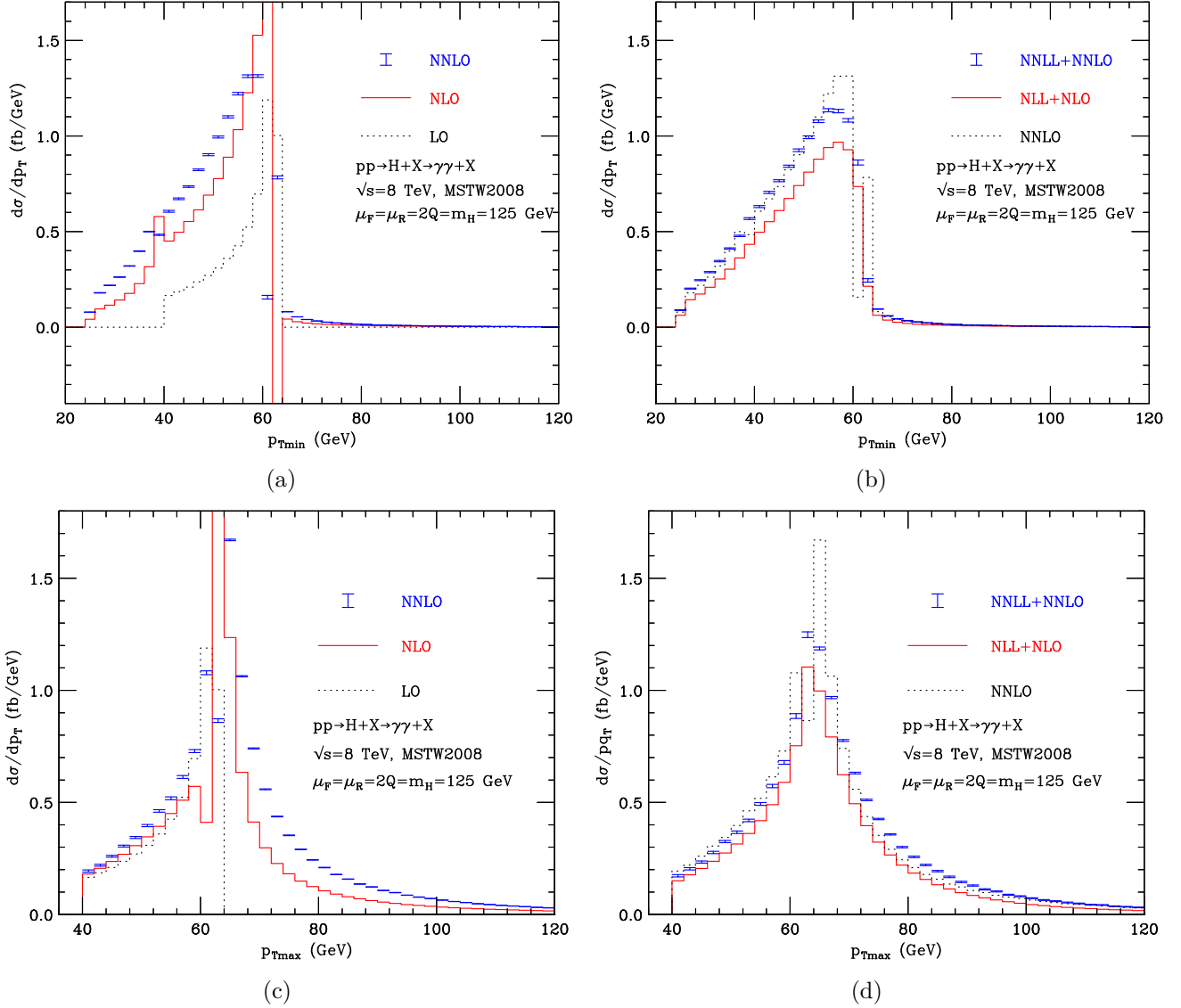
Figure 4: *Distributions in $p_{T\min}$ (a,b) and $p_{T\max}$ (c,d) for the $H \to \gamma\gamma$ signal at the LHC, obtained by fixed order (a,c) and resummed (b,d) calculations. In the right panels the fixed order NNLO result is also shown for comparison.*

As expected [49], resummed results do not suffer of such instabilities in the vicinity of the LO kinematical boundary; the resummed distributions are smooth and the shape is rather stable when going from NLL+NLO to NNLL+NNLO**.

An analogous perturbative instability is present in the $p_{T\min}$ distribution around $p_{T\min} \sim 40$ GeV at NLO and NNLO (see Fig. 4(a)). Such instability, which is not related to the use of the narrow width approximation, is due to the choice of asymmetric cuts for the photons. Beyond LO, the region $p_{T\min} < 40$ GeV opens up, and the step-like behaviour at LO leads to integrable logarithmic singularities at NLO and beyond. The resummed NLL+NLO and NNLL+NNLO

**We note that the small-p_T resummation we perform in this paper is not strictly the one needed to cure these logarithmic singularities [49]. Nonetheless, since our resummation provides a correct description of the Higgs boson kinematics, we do not expect that a rigorous treatment of these logarithmic singularities would lead to substantial numerical differences.

results are free of such perturbative instability.

Finally, a variable that is often studied is $\cos\theta^*$, where θ^* is the polar angle of one of the photons in the Higgs boson rest frame. Given the 4-momentum of the photon $p_\gamma = (m_H/2, \vec{p}_T^{\,\gamma}, p_z^\gamma)$ in the Higgs rest frame, the θ^* angle is defined as follows

$$|\cos\theta^*| = \frac{|p_z^\gamma|}{m_H/2};\tag{18}$$

considering the on-shell condition for the photon $p_T^{\gamma\,2} + p_z^{\gamma\,2} = (m_H/2)^2$ and that at the LO the p_T of the Higgs boson is zero, we can invert the on-shell condition, obtaining

$$|\cos\theta^*| = \sqrt{1 - \frac{4p_T^{\gamma\,2}}{m_H^2}}.\tag{19}$$

A cut on the photon transverse momentum p_T^γ implies a maximum value for $\cos\theta^*$ at LO. For example for $m_H = 125$ GeV and $p_T^\gamma \geq 40$ GeV we obtain

$$p_T^\gamma \geq 40 \text{ GeV} \quad \Rightarrow \quad |\cos\theta^*| \leq |\cos\theta_{\text{cut}}^*| \simeq 0.768.\tag{20}$$

At the NLO and NNLO the Higgs transverse momentum is non vanishing and events with $|\cos\theta^*| > |\cos\theta_{\text{cut}}^*|$ are kinematically allowed. In the region of the kinematical boundary higher-order perturbative distributions suffer of logarithmic singularities (as it happen for the photon distributions discussed above). In Fig. 5 we report both the distributions (normalized to unity) obtained by fixed order and the resummed calculations. We see that the resummed results are smooth in the region around the kinematical boundary. Away from such region, fixed order and resummed results show perfect agreement.
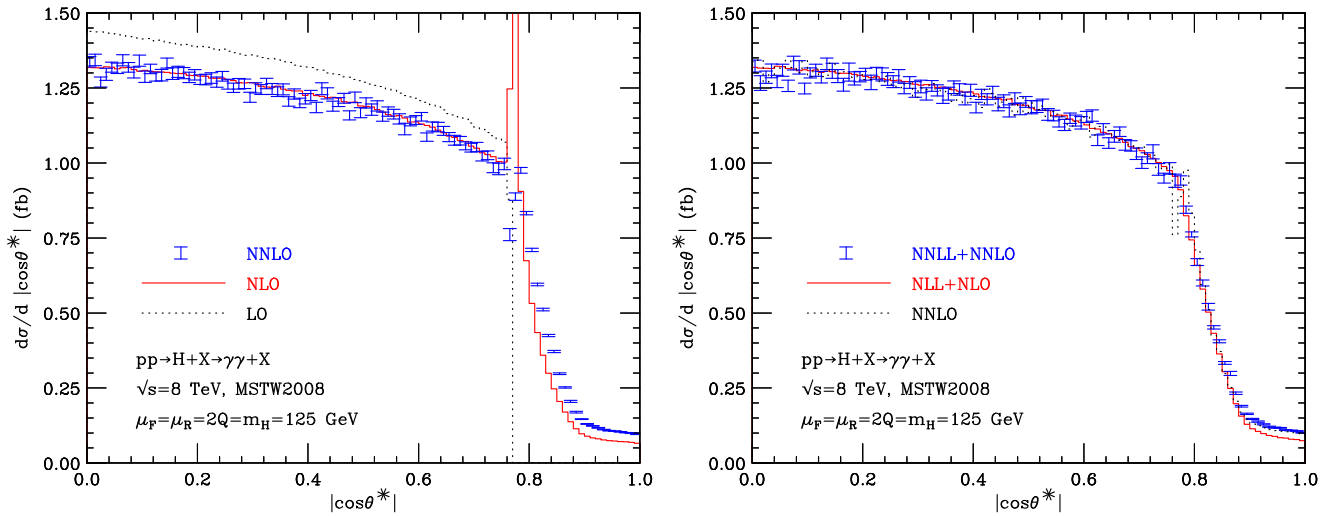

Figure 5: *Normalised $\cos\theta^*$ distribution at the LHC. On the left: LO, NLO and NNLO results. On the right: resummed predictions at NLL+NLO and NNLL+NNLO accuracy are compared with the NNLO result.*

3.3 $H \to WW \to l\nu l\nu$

We now consider the production of a SM Higgs boson with mass $m_H = 140$ GeV. The width is computed with the program HDECAY [45] to be $\Gamma_H = 8.11$ MeV. We consider the decay $W \to l\nu$ by assuming only one final state lepton combination. In order to isolate the possible signal some acceptance cuts are needed. Here we apply the following set of cuts [50]:

- the event should contain two opposite charged leptons having p_T larger than 20 GeV and in the central rapidity region $|\eta| < 2.5$;

- the missing p_T of the event should be larger than 30 GeV;

- the invariant mass of charged leptons should be larger than 12 GeV.

In Table 3 we report the fixed order and resummed predictions for the total and accepted cross section. We see that, also in this case, the inclusion of resummation does not lead to substantial differences on the accepted cross section. In Table 4 we report the accepted cross section for different scales. The scale uncertainty is about $\pm 17\%$ at NLL+NLO and NLO, whereas at NNLL+NNLO and NNLO it is reduced to $\pm 10\%$.

Cross section	NLO	NLL+NLO	NNLO	NNLL+NNLO
Total [fb]	61.58 ± 0.04	61.58 ± 0.04	76.94 ± 0.09	76.88 ± 0.19
With cuts [fb]	20.98 ± 0.03	20.90 ± 0.02	26.44 ± 0.10	26.32 ± 0.05
Efficiency [%]	34.0	33.9	34.4	34.2

Table 3: *Fixed order and resummed cross sections for $pp \to H + X \to WW + X \to l\nu l\nu + X$ before and after selection cuts.*

Cross section [fb]	NLO	NLL+NLO	NNLO	NNLL+NNLO
$(2Q = \mu_F = \mu_R) = m_H/2$	25.14 ± 0.03	25.13 ± 0.04	29.16 ± 0.17	29.05 ± 0.22
$(2Q = \mu_F = \mu_R) = m_H$	20.98 ± 0.03	20.90 ± 0.02	26.44 ± 0.10	26.32 ± 0.05
$(2Q = \mu_F = \mu_R) = 2m_H$	17.76 ± 0.02	18.26 ± 0.03	23.85 ± 0.07	24.14 ± 0.10

Table 4: *Fixed order and resummed accepted cross sections for $pp \to H+X \to WW+X \to l\nu l\nu+X$ at the LHC, for different choices of the scales.*

For each event, we classify the transverse momenta of the charged leptons according to their minimum and maximum value (as we did for the photon transverse momenta in $H \to \gamma\gamma$). In Fig. 6 we plot the corresponding distributions. We compare the resummed NLL+NLO and NNLL+NNLO predictions with the corresponding fixed order predictions at the LO, NLO and NNLO accuracy. We see that QCD corrections tend to make the distributions harder. Analogous effects are observed on the average transverse momentum spectrum of the W bosons, which is reported in Fig. 7. In particular, in order to quantitatively estimate the impact of the resummation, Figs. 6, 7 are organised in two panels. In the upper panels, we show the predictions obtained by different fixed order and resummed calculations. In the lower panel we plot (in red) the ratio NLL+NLO/NLO and (in blue) NNLL+NNLO/NNLO. From Fig. 6 we note that, in the peak

region, for both the p_{Tmin} and p_{Tmax} distributions, the resummed result is smaller by $5 - 10\%$ at NLL+NLO and by $2 - 4\%$ at NNLL+NNLO with respect to the corresponding fixed order prediction. In the intermediate region the resummation affects the results in the opposite direction, enhancing the cross section up to about 30% at NLL+NLO and 10% at NNLL+NNLO. The effects observed for the average p_T of the W bosons (see Fig. 7) are even more pronounced. These effects on the p_T spectra imply that the agreement between resummed and fixed order predictions we have observed in Table 3 cannot persist in general. When more restrictive cuts on the transverse momenta are applied, we anticipate non negligible effects from resummation.
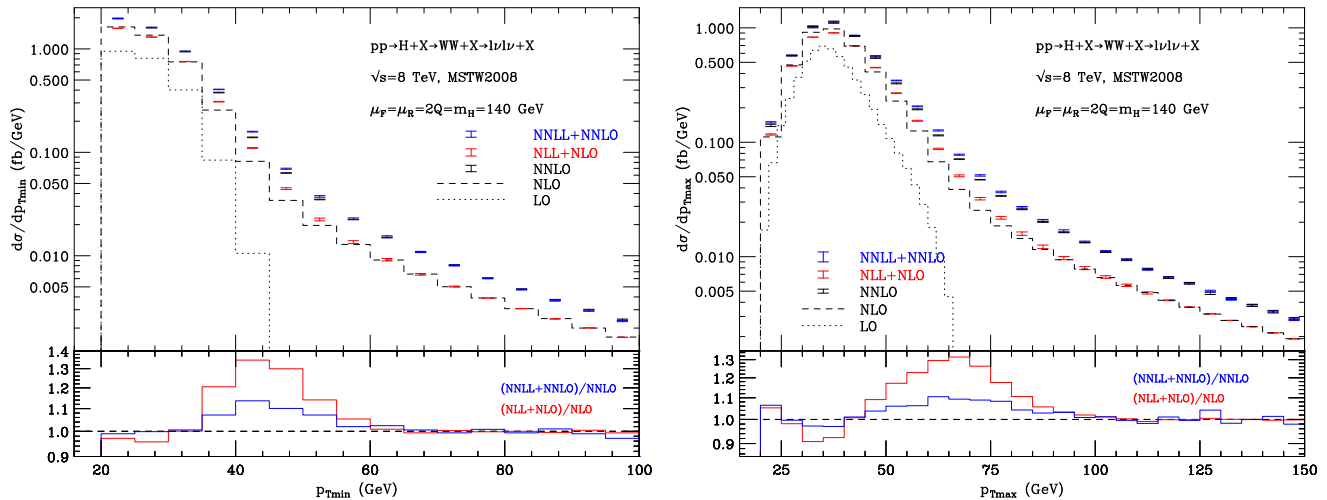

Figure 6: *Transverse momentum spectra of the lepton with minimum (left) and maximum (right) p_T for $pp \to H + X \to WW + X \to l\nu l\nu + X$ at the LHC. Resummed results at NLL+NLO and NNLL+NNLO accuracy are compared with fixed order predictions at LO, NLO and NNLO. The lower panels show the NNLL+NNLO result normalized to NNLO (solid) and the NLL+NLO result normalized to NLO (dashes).*

A very important discriminating variable for the $H \to WW \to l\nu l\nu$ decay channel is the azimuthal separation of the charged leptons in the transverse plane, $\Delta\phi$. As is well known [51], for the Higgs boson signal the leptons tend to be close in angle, thus the bulk of the events is produced at small $\Delta\phi$. Our results for the $\Delta\phi$ distribution are reported in Fig. 8. We can see that in the very small $\Delta\phi$ region ($\Delta\phi \lesssim 30^o$), there are less events than expected: this is an effect of the applied cuts. We notice that the steepness of the distributions increases when going from LO to NLO and from NLO to NNLO, and also increases when going from fixed order to resummed predictions, i.e. from NLO to NLL+NLO and from NNLO to NNLL+NNLO. This fact can be interpreted as follows: when the Higgs boson p_T distribution is harder the final state leptons tend to be more boosted in the transverse plane and thus their transverse angular separation becomes smaller. As a consequence the steepness of the $\Delta\phi$ distribution increases and the efficiency of cuts slightly increases with the perturbative accuracy.

3.4 $\quad H \to ZZ \to \mu^+\mu^-e^+e^-$

We now consider the production of a Higgs boson with mass $m_H = 150$ GeV. The width is computed with the program HDECAY [45] to be $\Gamma_H = 16.9$ MeV. In this mass region, the
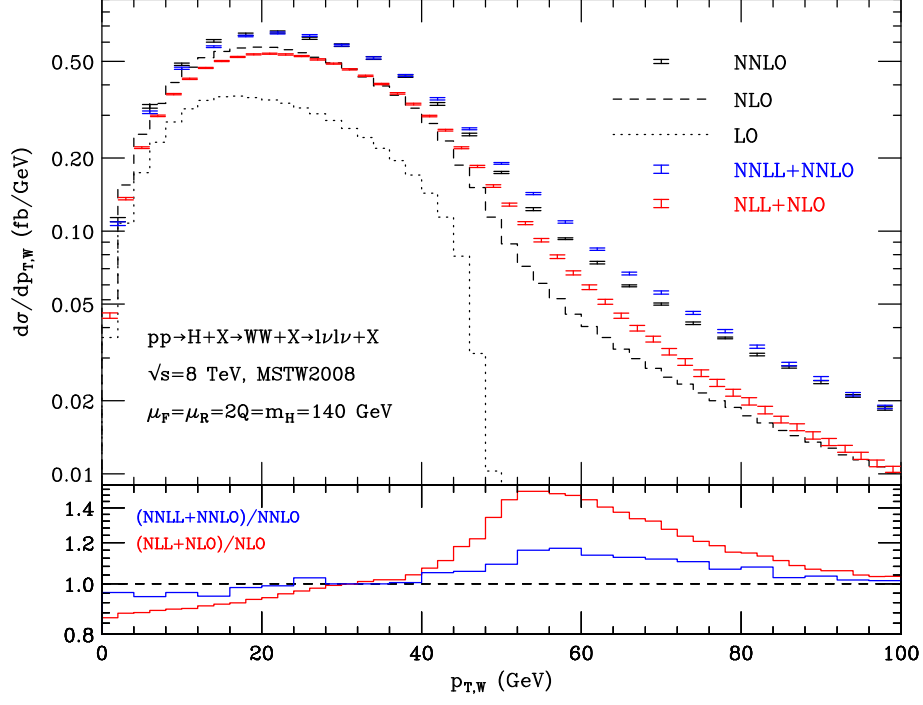
Figure 7: *Average transverse momentum spectrum of the W bosons for* $pp \rightarrow H+X \rightarrow WW+X \rightarrow l\nu l\nu + X$ *at the LHC when cuts are applied. Resummed results at NLL+NLO and NNLL+NNLO accuracy are compared with fixed order predictions at LO, NLO and NNLO. The lower panel shows the NNLL+NNLO result normalized to NNLO (solid) and the NLL+NLO result normalized to NLO (dashes).*
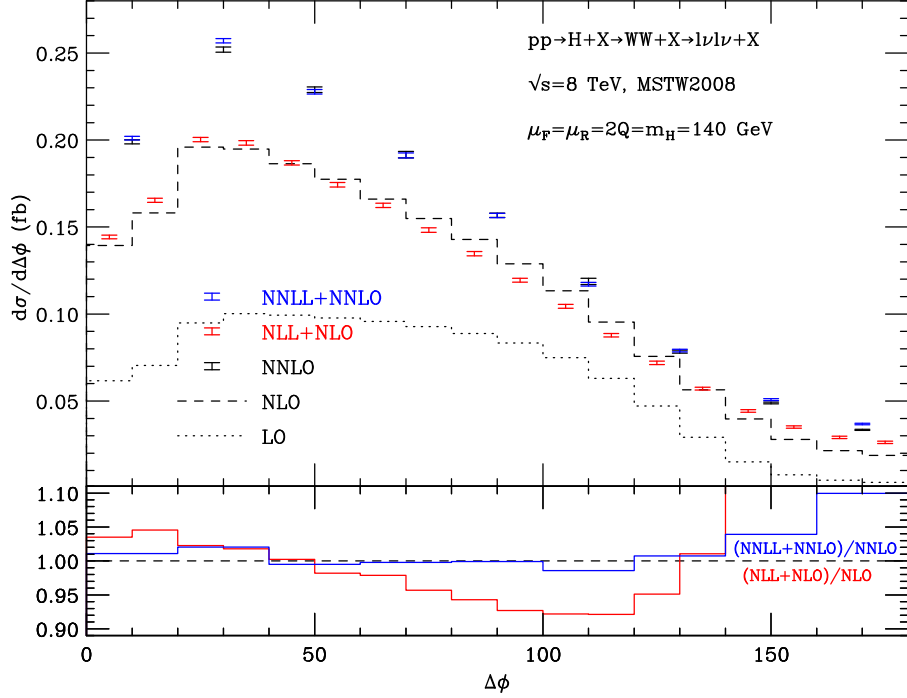

Figure 8: *Same as in Fig. 7 but for the* $\Delta\phi$ *distribution.*

$H \rightarrow ZZ \rightarrow 4l$ decay mode is not the dominant decay channel, but still it can provide a clean and useful four lepton signature. In the following we consider the decay of the Higgs boson in two different lepton pairs.

We consider the following cuts [50]:

- the event should contain two pairs of opposite charged leptons

- each lepton must have p_T larger than 5 GeV and should be in the central rapidity region $|\eta| < 2.5$;

- for each lepton pair, the closest (m_1) and the next-to-closest (m_2) to m_Z are found; then m_1, m_2 are required to be $m_1 > 50$ GeV and $m_2 > 12$ GeV.

Note that an isolation cut on the leptons is generally required. For example, a typical isolation is to require the total transverse energy E_T in a cone of a given radius R around each lepton to be smaller than a fraction of the lepton p_T. As in the $H \rightarrow \gamma\gamma$ decay mode isolation cuts cannot be applied, because in the resummed calculation we are necessarily inclusive over the QCD radiation accompanying the Higgs boson. By using the fixed order `HNNLO` code we have checked that the numerical effect of the isolation cuts is extremely small.

In Tab. 5 we compare the effects of cuts on the inclusive cross sections. As in the $H \rightarrow \gamma\gamma$ and $H \rightarrow WW$ decays, the efficiency slightly improves increasing the perturbative accuracy, but no substantial effects from resummation are observed. In Tab. 6 the accepted cross section for different choices of the scales is reported. At the NLL+NLO (NLO) accuracy the ensuing scale uncertainty is $\sim \pm 15\%$ ($\pm 17\%$) and at the NNLL+NNLO (NNLO) it is $\sim \pm 9\%$ ($\pm 10\%$).

Cross section	NLO	NLL+NLO	NNLO	NNLL+NNLO
Total [fb]	1.720 ± 0.001	1.720 ± 0.002	2.142 ± 0.004	2.156 ± 0.006
With cuts [fb]	1.127 ± 0.001	1.136 ± 0.001	1.413 ± 0.005	1.427 ± 0.003
Efficiency [%]	65.6	66.0	66.0	66.2

Table 5: *Fixed order and resummed cross section for $pp \rightarrow H + X \rightarrow ZZ + X \rightarrow \mu^+\mu^- e^+ e^- + X$ cross section before and after geometrical acceptance cuts.*

Cross section [fb]	NLO	NLL+NLO	NNLO	NNLL+NNLO
$(2Q = \mu_F = \mu_R) = m_H/2$	1.350 ± 0.001	1.350 ± 0.004	1.572 ± 0.007	1.570 ± 0.006
$(2Q = \mu_F = \mu_R) = m_H$	1.127 ± 0.001	1.136 ± 0.001	1.413 ± 0.005	1.427 ± 0.003
$(2Q = \mu_F = \mu_R) = 2m_H$	0.954 ± 0.001	0.992 ± 0.003	1.273 ± 0.003	1.310 ± 0.003

Table 6: *Fixed order and resummed accepted cross sections for $pp \rightarrow H + X \rightarrow ZZ + X \rightarrow \mu^+\mu^- e^+ e^- + X$ at the LHC, for different choices of the scales.*

In Fig. 9 we plot the four p_T spectra of the final state leptons. Note that at LO the p_{T1}, p_{T2} are kinematically bounded by $m_H/2$, whereas $p_{T3} < m_H/3$ and $p_{T4} < m_H/4$. In the vicinity of such boundaries, higher order QCD predictions may in principle develop perturbative instabilities. On the other hand, contrary to what happens in the $H \rightarrow \gamma\gamma$ decay mode, the LO distributions

smoothly reach their kinematical boundary and we do not observe perturbative instabilities beyond the LO. The impact of resummation is to make the transverse momentum spectra harder. The resummation effects are more pronounced in the leading lepton transverse momentum spectrum (see Fig. 9(a)) and less evident in the softest lepton spectrum (see Fig. 9(d)).
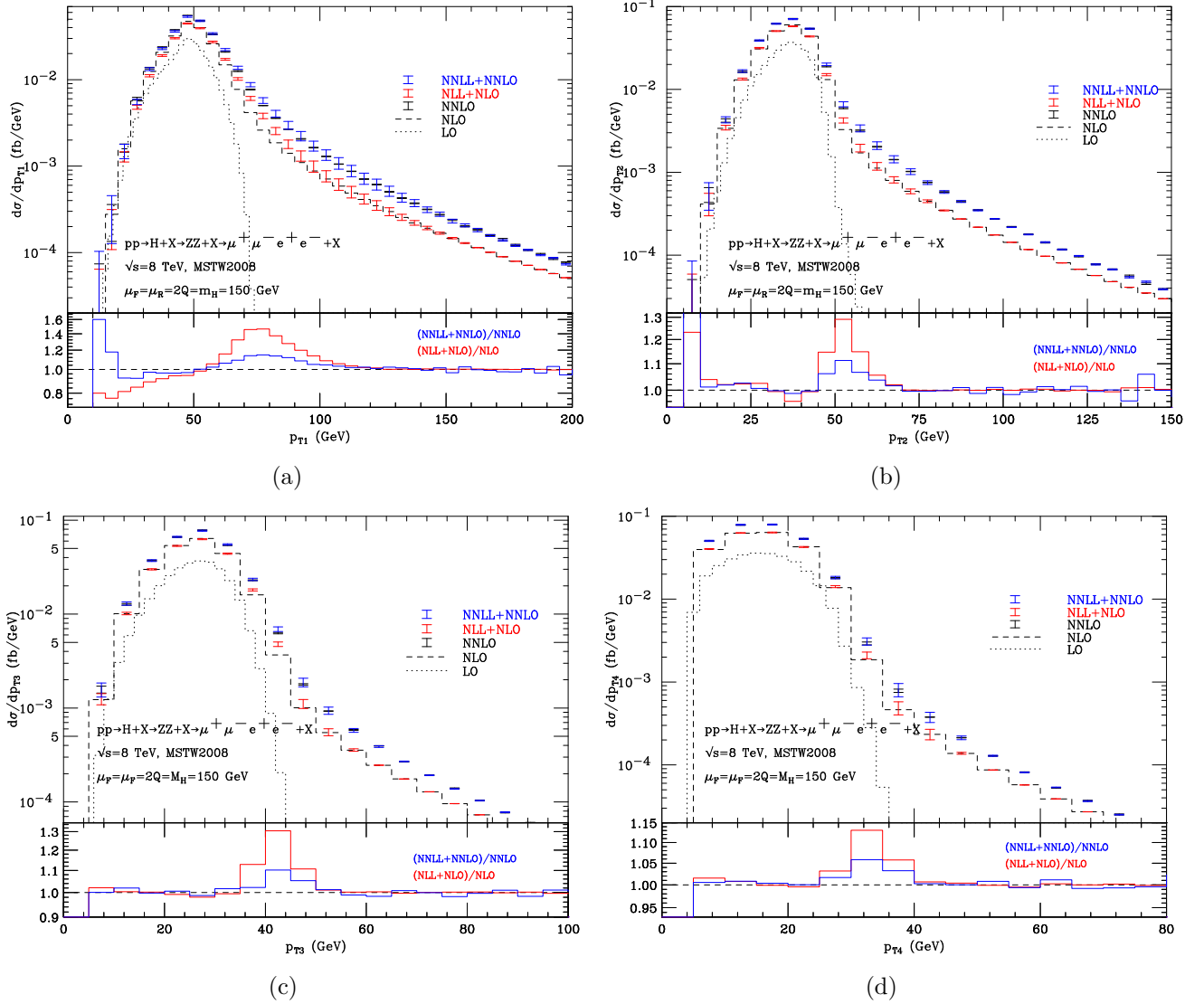

Figure 9: *Transverse momentum spectra of the final state leptons for $pp \to H + X \to ZZ + X \to \mu^+\mu^-e^+e^- + X$ at the LHC, when cuts are applied. The lepton p_T are ordered according to decreasing p_T. They are obtained through fixed order (black) and resummed (red and blue) calculations. The lower panels show the ratios between resummed and fixed order predictions.*

In Fig. 10 we show the average p_T distribution of the two Z bosons. The comments are analogous to those for previous distributions: QCD radiation tends to make the distribution harder and the fixed order results are again recovered at large transverse momentum.
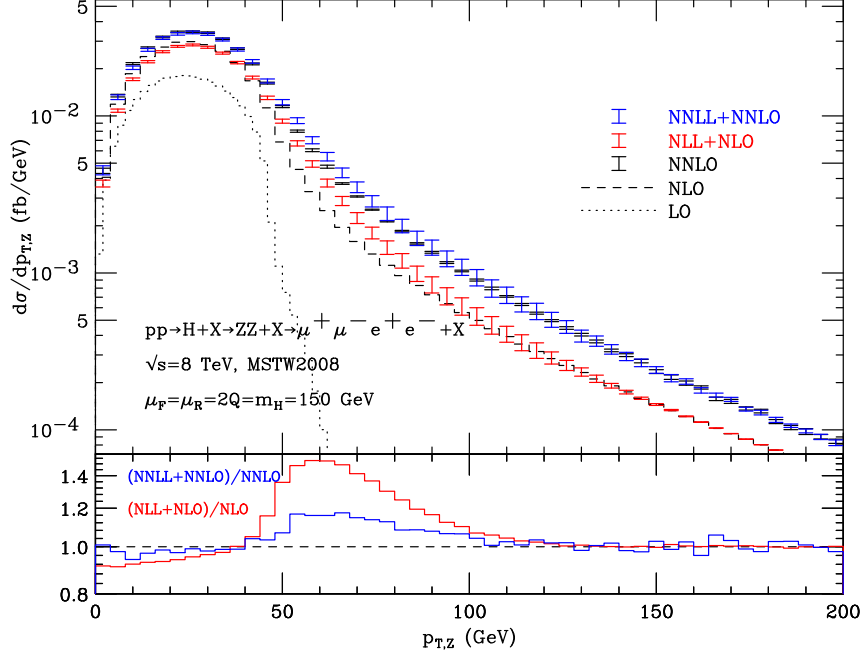
Figure 10: *Average p_T spectrum of the Z bosons for $pp \to H + X \to ZZ + X \to \mu^+\mu^-e^+e^- + X$ at the LHC, when cuts are applied. Resummed results at NLL+NLO and NNLL+NNLO accuracy are compared with fixed order predictions at LO, NLO and NNLO. The lower panel shows the NNLL+NNLO result normalized to NNLO (solid) and the NLL+NLO result normalized to NLO (dashes).*

3.5 Discussion

As explained at the end of Sec. 2 our numerical program implements a smooth switching procedure between the resummed and fixed order results (see Eqs. (13) and (15)). The numerical parameters in Eq. (13) can be consistently chosen such that the integral of our NLL+NLO and NNLL+NNLO resummed result still reproduces well the NLO and NNLO inclusive cross sections. We have studied the uncertainty inherent in such switching procedure. We find that for other forms of the switching function and different choices of the corresponding parameters the numerical effects on the final results remain within the uncertainties estimated by performing variations of the resummation scale Q.

We conclude this Section by adding few comments on the work of Ref. [52]. In this paper the RESBOS generator [53], which is based on the classical b-space resummation formalism of Ref. [27], is used to perform a study of transverse momentum resummation effects in the $H \to WW \to l\nu l\nu$ and $H \to ZZ \to 4l$ channels at the Tevatron and the LHC. The resummed calculation in the low p_T region is matched to the $\mathcal{O}(\alpha_S^3)$ result at high p_T. Besides the differences in the resummation formalism (see Ref. [31] for a detailed discussion) there are a few differences with respect to the work presented here. Our calculation implements the value of the coefficient $A^{(3)}$ from Ref. [41], whereas in Ref. [52] the authors use the result of Ref. [54] that applies to threshold resummation. The calculation of Ref. [52] does not include the hard collinear coefficients $\mathcal{H}^{(2)}$ presented in Ref. [40] and thus its accuracy, with our notations, is essentially limited to NLL+NLO (plus some of the NNLL terms). Finally, the calculation of Ref. [52] does not exploit a unitarity constraint

on the total cross section, and thus the normalization of the ensuing resummed spectra is not constrained.

In their phenomenological study, when comparing resummed and fixed-order NLO predictions, the authors of Ref. [52] find significant resummation effects. The reason is twofold. First, the cuts that are considered in Ref. [52] are more restrictive, and thus resummation effects are made more relevant. Second, the comparison is done one order lower than ours (i.e. the NLL+NLO resummed prediction is compared to the fixed order NLO result) where we also find more significant distortions of the relevant kinematical distributions (see Figs. 6-10).

4 Summary and outlook

We have presented a calculation of the NNLL+NNLO cross section for Higgs boson production at the LHC, in the decay modes $H \to \gamma\gamma$, $H \to WW \to l\nu l\nu$ and $H \to ZZ \to 4$ leptons. The calculation takes into account some illustrative experimental cuts analogous to the ones designed to isolate the Higgs boson signal.

Our calculation is implemented in the numerical program `HRes` [37]. The present version of the program includes the most relevant decay modes of the Higgs boson, namely, $H \to \gamma\gamma$, $H \to WW \to l\nu l\nu$ and $H \to ZZ \to 4$ leptons. In the latter case it is possible to choose between $H \to ZZ \to \mu^+\mu^- e^+ e^-$ and $H \to ZZ \to e^+ e^- e^+ e^-$, which includes the appropriate interference contribution. The user can apply all the required cuts on the Higgs boson and its decay products and plot the corresponding distributions in the form of bin histograms. These features should make our program a useful tool for Higgs searches and studies at the Tevatron and the LHC.

The calculations performed through `HRes` strictly implement the large M_t approximation. This is known to be a good approximation for the p_T spectrum of the Higgs boson, provided that p_T is not too large ($p_T \lesssim M_t$) [55]. For very large transverse momenta the large-M_t approximation is bound to fail, since the QCD radiation accompanying the Higgs boson becomes sensitive to the heavy-quark loop. The inclusion of top and bottom mass effects up to $\mathcal{O}(\alpha_S^3)$ in `HRes` is feasible and is left to future work. Another limitation of the calculation is that we completely neglect radiative corrections in the Higgs boson decay. The full QCD+EW corrections to the decay modes $H \to WW(ZZ) \to 4$ leptons are available [56] and we plan to include these effects in a future version of the program.

Acknowledgements

References

[1] F. Englert and R. Brout, Phys. Rev. Lett. **13** (1964) 321; P. W. Higgs, Phys. Lett. **12** (1964) 132, Phys. Rev. Lett. **13** (1964) 508.

[2] [ATLAS Collaboration], arXiv:1202.1408 [hep-ex].

[3] S. Chatrchyan *et al.* [CMS Collaboration], arXiv:1202.1488 [hep-ex].

[4] [TEVNPH (Tevatron New Phenomena and Higgs Working Group) and CDF and D0 Collaborations], *Combined CDF and D0 Search for Standard Model Higgs Boson Production with up to 10 fb^{-1} of Data*, FERMILAB-CONF-12-065-E.

[5] H. M. Georgi, S. L. Glashow, M. E. Machacek and D. V. Nanopoulos, Phys. Rev. Lett. **40** (1978) 692.

[6] S. Dawson, Nucl. Phys. B **359** (1991) 283.

[7] A. Djouadi, M. Spira and P. M. Zerwas, Phys. Lett. B **264** (1991) 440.

[8] M. Spira, A. Djouadi, D. Graudenz and P. M. Zerwas, Nucl. Phys. B **453** (1995) 17.

[9] R. V. Harlander and W. B. Kilgore, Phys. Rev. Lett. **88** (2002) 201801.

[10] C. Anastasiou and K. Melnikov, Nucl. Phys. B **646** (2002) 220.

[11] V. Ravindran, J. Smith and W. L. van Neerven, Nucl. Phys. B **665** (2003) 325.

[12] S. Marzani, R. D. Ball, V. Del Duca, S. Forte and A. Vicini, Nucl. Phys. B **800** (2008) 127.

[13] R. V. Harlander and K. J. Ozeren, Phys. Lett. B **679** (2009) 467.

[14] R. V. Harlander and K. J. Ozeren, JHEP **0911** (2009) 088.

[15] R. V. Harlander, H. Mantler, S. Marzani and K. J. Ozeren, Eur. Phys. J. C **66** (2010) 359.

[16] A. Pak, M. Rogal and M. Steinhauser, Phys. Lett. B **679** (2009) 473.

[17] A. Pak, M. Rogal and M. Steinhauser, JHEP **1002** (2010) 025.

[18] S. Catani, D. de Florian and M. Grazzini, JHEP **0201** (2002) 015.

[19] C. Anastasiou, K. Melnikov and F. Petriello, Phys. Rev. Lett. **93** (2004) 262002, Nucl. Phys. B **724** (2005) 197.

[20] C. Anastasiou, G. Dissertori and F. Stockli, JHEP **0709** (2007) 018.

[21] S. Catani and M. Grazzini, Phys. Rev. Lett. **98** (2007) 222002.

[22] M. Grazzini, JHEP **0802** (2008) 043.

[23] Y. L. Dokshitzer, D. Diakonov and S. I. Troian, Phys. Lett. B **79** (1978) 269, Phys. Rep. **58** (1980) 269.

[24] G. Parisi and R. Petronzio, Nucl. Phys. B **154** (1979) 427.

[25] G. Curci, M. Greco and Y. Srivastava, Nucl. Phys. B **159** (1979) 451.

[26] J. C. Collins and D. E. Soper, Nucl. Phys. B **193** (1981) 381 [Erratum-ibid. B **213** (1983) 545]; Nucl. Phys. B **197** (1982) 446.

[27] J. C. Collins, D. E. Soper and G. Sterman, Nucl. Phys. B **250** (1985) 199.

[28] J. Kodaira and L. Trentadue, Phys. Lett. B **112** (1982) 66, report SLAC-PUB-2934 (1982), Phys. Lett. B **123** (1983) 335.

[29] S. Catani, E. D'Emilio and L. Trentadue, Phys. Lett. B **211** (1988) 335.

[30] S. Catani, D. de Florian and M. Grazzini, Nucl. Phys. B **596** (2001) 299.

[31] G. Bozzi, S. Catani, D. de Florian and M. Grazzini, Nucl. Phys. B **737** (2006) 73.

[32] S. Catani and M. Grazzini, Nucl. Phys. B **845** (2011) 297.

[33] D. de Florian and M. Grazzini, Phys. Rev. Lett. **85** (2000) 4678, Nucl. Phys. B **616** (2001) 247.

[34] D. de Florian, M. Grazzini and Z. Kunszt, Phys. Rev. Lett. **82** (1999) 5209.

[35] V. Ravindran, J. Smith and W. L. Van Neerven, Nucl. Phys. B **634** (2002) 247.

[36] C. J. Glosser and C. R. Schmidt, JHEP **0212** (2002) 016.

[37] `http://theory.fi.infn.it/grazzini/codes.html`

[38] G. Bozzi, S. Catani, D. de Florian and M. Grazzini, Nucl. Phys. B **791** (2008) 1.

[39] D. de Florian, G. Ferrera, M. Grazzini and D. Tommasini, JHEP **1111** (2011) 064.

[40] S. Catani and M. Grazzini, report ZU-TH-12-11 (arXiv:1106.4652 [hep-ph]).

[41] T. Becher and M. Neubert, Eur. Phys. J. C **71** (2011) 1665.

[42] R. P. Kauffman, Phys. Rev. D **45** (1992) 1512.

[43] C. P. Yuan, Phys. Lett. B **283** (1992) 395.

[44] A. D. Martin, W. J. Stirling, R. S. Thorne and G. Watt, Eur. Phys. J. C **63** (2009) 189.

[45] A. Djouadi, J. Kalinowski and M. Spira, Comput. Phys. Commun. **108** (1998) 56.

[46] [ATLAS Collaboration], arXiv:1202.1414 [hep-ex].

[47] M. Vesterinen and T. R. Wyatt, Nucl. Instrum. Meth. A **602** (2009) 432.

[48] A. Banfi, M. Dasgupta and R. M. Duran Delgado, JHEP **0912** (2009) 022.

[49] S. Catani and B. R. Webber, JHEP **9710** (1997) 005.

[50] S. Dittmaier, S. Dittmaier, C. Mariotti, G. Passarino, R. Tanaka, S. Alekhin, J. Alwall and E. A. Bagnaschi *et al.*, arXiv:1201.3084 [hep-ph].

[51] M. Dittmar and H. K. Dreiner, Phys. Rev. D **55** (1997) 167.

[52] Q. -H. Cao and C. -R. Chen, Phys. Rev. D **76** (2007) 073006.

[53] C. Balazs and C. P. Yuan, Phys. Lett. B **478** (2000) 192.

[54] S. Moch, J. A. M. Vermaseren and A. Vogt, Nucl. Phys. B **688** (2004) 101.

[55] U. Baur and E. W. N. Glover, Nucl. Phys. B **339** (1990) 38.

[56] A. Bredenstein, A. Denner, S. Dittmaier and M. M. Weber, Phys. Rev. D **74** (2006) 013004, JHEP **0702** (2007) 080.